

Article

An Evaluation of the Atmospheric Instability Effect on Wildfire Danger Using ERA5 over the Iberian Peninsula

Luana C. Santos ¹, Miguel M. Lima ¹, Virgílio A. Bento ¹, Sílvia A. Nunes ¹, Carlos C. DaCamara ¹, Ana Russo ¹, Pedro M. M. Soares ¹ and Ricardo M. Trigo ^{1,2,*}

¹ Faculdade de Ciências, Instituto Dom Luiz (IDL), Universidade de Lisboa, 1749-016 Lisboa, Portugal

² Departamento de Meteorologia, Universidade Federal do Rio de Janeiro, Rio de Janeiro 21941-919, Brazil

* Correspondence: rmtrigo@ciencias.ulisboa.pt

Abstract: The Fire Weather Index (FWI) is used to assess meteorological fire danger worldwide. It has been argued that it lacks an atmospheric instability term. A new enhanced FWI (FWIe) was recently developed incorporating atmospheric instability in the form of the Continuous Haines Index (CHI). Here, the first climatological and evolution analysis of these indexes was performed using ERA5 data for the 1980–2020 period. There was a prevalence of higher values over central Iberia; these were heavily modulated by the climate types, topography, and land cover. Southwest and east Iberia suffered the greatest decadal increases in all three indexes. Relating both indexes to occurrences detected by satellite, through fire radiative power (FRP), showed that FWIe provided an improved meteorological fire danger assessment in higher-risk conditions. This showed that greater-risk observations were more prone to be affected by atmospheric instability than lower-danger observations. Case studies for the 2017 central Portugal and 2003 and 2018 Monchique wildfires were additionally conducted to verify these conclusions. This work points to the usefulness of FWIe when/where atmospheric instability may play a critical role in the development of wildfires, which may contribute to a more focused deployment of suppression mechanisms by the authorities.

Keywords: Fire Weather Index; Continuous Haines Index; wildfires; Iberian Peninsula; fire radiative power; ERA5



Citation: Santos, L.C.; Lima, M.M.; Bento, V.A.; Nunes, S.A.; DaCamara, C.C.; Russo, A.; Soares, P.M.M.; Trigo, R.M. An Evaluation of the Atmospheric Instability Effect on Wildfire Danger Using ERA5 over the Iberian Peninsula. *Fire* **2023**, *6*, 120. <https://doi.org/10.3390/fire6030120>

Academic Editor: Grant Williamson

Received: 1 February 2023

Revised: 1 February 2023

Accepted: 11 March 2023

Published: 14 March 2023



Copyright: © 2023 by the authors. Licensee MDPI, Basel, Switzerland. This article is an open access article distributed under the terms and conditions of the Creative Commons Attribution (CC BY) license (<https://creativecommons.org/licenses/by/4.0/>).

1. Introduction

Wildfires are important extreme events that affect world ecosystems and human populations [1–3]. Wildfire behavior, namely the rate of spread and burning patterns, depends on a variety of factors, including ignition, topography, land cover, fire management and suppression policies, and weather conditions [1,4–6].

In the past few decades, several studies have analyzed the evolution of fire regimes over different regions of the world, taking into consideration ongoing global climate change [1,7–10]. In this regard, the Mediterranean basin has attracted special attention since it is recurrently subject to large wildfires, due to its warm and dry summers together with persistent heat spells [5,6,11,12]. Within the Mediterranean, the Iberian Peninsula (IP) is the area most affected by wildfires, representing more than 60% (about 11 million ha) of the total burned area of the five southern European Union (EU) Member States (i.e., Portugal, Spain, France, Italy, and Greece) [10,13]. This is even more relevant since Portugal and northwestern Spain (Galicia) is one of the most wildfire-prone areas in Europe [10], and future climate projections point to a substantial increase in fire danger for the next few decades [1,7–10]. Human-related factors also contribute to the existence of wildfires, with the Mediterranean regions showing the largest proportion of human-caused fires in the world, including the intentional or negligent use of fire or even inappropriate forestry management [14,15].

The highly favorable climate conditions observed in the IP are linked to the three main types of wildfires which often occur in the region, namely wind-driven, topo-graphic, and

plume-dominated or convective fires [16–18]. Wind-driven wildfires strongly depend on wind intensity and direction, with small changes in landscape and topography having virtually no impact on fire propagation [19]. Topographic fires are highly dependent on local-scale winds caused by differential solar heating (i.e., slope or valley winds and sea breezes), showing a strong day–night intensity change [20]. Plume-dominated (convective) fires are characterized by the presence of intense atmospheric instability allied with the accumulation and availability of fuels for fire development, normally being more intense (energetic) and with unpredictable behavior [21].

Several methods have been proposed to assess meteorological fire danger in different regions using the Canadian Forest Fire Weather Index System (CFFWIS) [5,22,23]. Initially developed for use in the forests of Canada, CFFWIS is composed of six subindexes, namely three fuel moisture codes with a memory component (the Fine Fuel Moisture Code; the Duff Moisture Code; and the Drought Code); two fire behavior indexes based on the aforementioned codes and wind intensity (the Initial Spread Index and the Build-Up Index); and the Fire Weather Index (FWI), which results from the combination of the previous two indexes and is a numeric rating of fire intensity. A complete and thorough description of these indices can be found in Van Wagner [23]. An operational advantage of CFFWIS is that its components solely depend on daily weather observations, usually taken at local noon time, namely air temperature and relative humidity (RH), wind speed, and accumulated daily precipitation. Since the late 1980s and early 1990s, the FWI has been used as a meteorological fire index in a large variety of regions of the world and has proven to be especially suitable for assessing meteorological danger in the Mediterranean basin [5,24–26].

When characterizing plume-dominated wildfires, atmospheric instability is a crucial factor that is not accounted for by the FWI. With the intent of including the effect of atmospheric instability on wildfires, Haines [27] proposed a Lower Atmospheric Severity Index composed of a stability component, which is based on the difference between the absolute temperatures at two prescribed pressure levels chosen based on local surface elevation and a moisture component, corresponding to the lower-level difference between the absolute and dew-point temperatures. The index has since been revised in the form of the so-called Continuous Haines Index (CHI), which has been regularly used in the past decade [28,29]. The CHI requires a dry atmosphere and a steep lapse rate at the lower atmospheric level. If a situation of moist air at a lower level is present, the rising parcel reaches a low lifting condensation level, favorable to the development of storms with heavy rainfall [30]. In a recent study, Pinto et al. [18] proposed an enhanced version of FWI, hereafter FWI_e, that explicitly incorporates CHI into the traditional FWI.

To the best of our knowledge, there has been no comprehensive analysis of the relationship between atmospheric instability and wildfire danger indexes. The main goal of this study was to produce a climatological characterization of CHI, FWI, and FWI_e over the IP based on state-of-the-art reanalysis ERA5 data provided by the European Centre for Medium-Range Weather Forecasts (ECMWF) [31]. The study then focused on the large fire events that took place in 2003, 2017, and 2018 in Portugal and for each event, the performances of FWI and FWI_e were compared. This analysis allowed us to assess the usefulness of FWI_e in regions where and during periods when atmospheric instability plays a decisive role in the development of wildfires, contributing to a more efficient deployment of suppression activities.

2. Data and Methods

2.1. Study Region

This study focused on the Iberian Peninsula spanning the period between 1980 and 2020. The regionalization described in Sousa et al. [32] and Trigo et al. [33] was adopted here to divide the area into four clusters (Figure 1) with characteristic normalized burnt area behaviors, namely: a northwestern cluster aggregating the northern half of Portugal and the extreme northwest of Spain (NW), which is the most fire-prone cluster of the

entire study region with large fire activity in August; a southwestern cluster including the southern and interior regions of Portugal and central and southwestern Spain (SW), which is the second most fire-prone cluster in the region, with fire activity mostly prevailing in the summer months; an eastern cluster including the coast and pre-coastal areas east of Gibraltar up to the Pyrenees (E), which presents a higher danger of fire at the beginning of summer; and a northern cluster corresponding to regions over the mountainous sectors of northern Spain, such as the Asturias, Cantabria, and Basque Country (N), which is the least dangerous region with two moderate peaks of fire activity taking place in March and September (Figure 1).

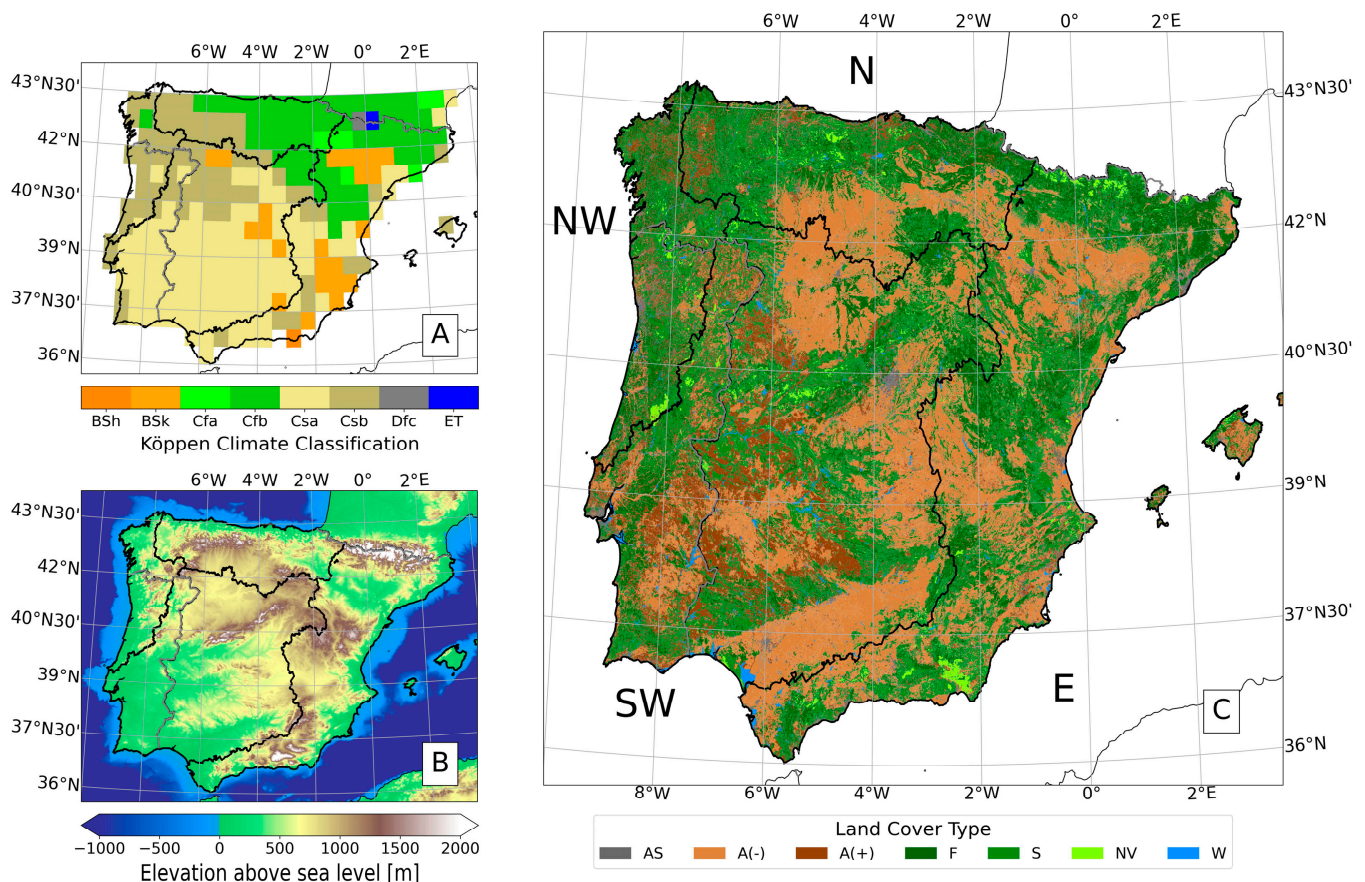


Figure 1. Detailed views of the study region including (A) Köppen climate types, as follows: BSh—hot semi-arid, BSk—cold semi-arid, Cfa—humid subtropical, Cfb—temperate oceanic, Csa—hot summer Mediterranean, Csb—warm summer Mediterranean, Dfc—subarctic, Et—tundra; (B) topography; and (C) land cover types, labeled as follows: AS—artificial surfaces, A(−)—agricultural (less forested), A(+)—agricultural (more forested), F—forest, S—shrub, NV—no vegetation, W—water. In each subplot, the clusters are drawn (in black) as well as the borders (in grey) of Portugal and Spain.

The study region comprised the Iberian Peninsula and is shown in Figure 1, where the Köppen climate types (Figure 1A), topography (Figure 1B), and land cover types (Figure 1C) are also detailed. The Köppen climate types (Figure 1A) for the IP were retrieved from Chen and Chen [34], showing that the IP mainly presents mild, temperate, and dry climate types with dry summers, while the northeastern area is humid all year long. The topography of the study region (Figure 1B) was retrieved from Smith and Sandwell [35], with most of southwestern Iberia being flat and presenting low values of altitude, whereas central, eastern, north, and northeastern Iberia includes large mountain ranges, peaking at nearly 3500 m, with most areas being below 1000 m. Land cover types were retrieved from the Copernicus Land Monitoring Service, CORINE Land Cover (CLC) 2018 [36], derived from satellite imagery obtained at different times during 2017 (e.g., forest types were retrieved

during the July–August period, since this land cover is more developed at this time of the year), with an approximate resolution of 100 m. The spatial distribution of land cover types revealed a close connection to that of the topography, with agricultural cover over much of the mountainous slopes and river valleys of the Peninsula. In the main mountain ranges located in the central and northwestern sectors of the Peninsula, there is a prevalence of forested areas. In central Portugal, a scar of no vegetation is visible, to which the 2017 summer wildfires contributed substantially [37]; however, the October wildfires are not visible due to the time of retrieval for this land cover type (July–August).

2.2. Reanalysis Data

Surface and atmospheric data were retrieved from the 5th generation of the European Centre for Medium-Range Weather Forecasts (ECMWF) global reanalysis (ERA5) [31], available in a $0.25^\circ \times 0.25^\circ$ spatial grid, to calculate CHI, FWI, and FWIe. For the computation of these indexes, we retrieved relative humidity (RH) at 850 hPa, temperature at 2 m and 700 and 850 hPa, the dew-point temperature at 2 m, U and V wind components at 10 m, and accumulated daily precipitation (computed from hourly values). All fields refer to 12 UTC.

2.3. Continuous Haines Index

We elected to use reasonable atmospheric levels to evaluate the CHI considering the average topography of the IP [38]; thus, we chose to use 850–700 hPa. The CHI is defined as:

$$CA = (T_{850} - T_{700})/2 - 2 \quad (1)$$

$$CB = \min(T_{850} - T_{d850}, 30)/3 - 1 \quad (2)$$

$$\text{If } CB > 5, \text{ then: } CB = 5 + (CB - 5)/2$$

$$CHI = CA + CB \quad (3)$$

where T_{700} and T_{850} are the absolute temperature values at 700 and 850 hPa, respectively, and T_{d850} is the dew-point temperature at 850 hPa. The $\min(T_{850} - T_{d850}, 30)$ term in Equation (2) indicates that an upper bound of 30°C was defined for the difference between the temperature and dew-point temperature at 850 hPa. The dew-point temperature (T_d) was computed from T and RH according to the Magnus formula, which yields a conversion between relative humidity and dew-point temperature with a relative error lower than 0.4% over the range $-40^\circ\text{C} \leq T \leq 50^\circ\text{C}$ [39]. Daily values of the CHI for the IP spanning the study period of 1980–2020 were computed according to relations (1)–(3) using reanalysis data from ERA5.

2.4. Fire Weather Index and Enhanced Fire Weather Index

As with CHI, the FWI system indexes were calculated for the IP spanning the full period using reanalysis data from ERA5. Daily values of the FWI were obtained following the source code of Wang et al. [26], with RH obtained from T and T_d using the Magnus formula [39].

In this study, we computed the enhanced FWIe using the code made available by Pinto et al. [18]. This calculation was highly dependent on the region of study and to a lesser degree on the temporal window studied. In the case of higher-than-usual CHI values, i.e., in the case of high atmospheric instability in the lower levels, FWIe presents larger values than FWI; conversely, in the case of a lower-than-usual CHI, the FWIe has lower values relative to the FWI [18].

2.5. Fire Radiative Power

Information about the intensity and severity of fires was based on the power released by the event, which was determined according to the fire radiative power (FRP) using the MODIS Collection 6 Active Fire Product [40] with data availability from 2001 to 2020 (<https://earthdata.nasa.gov>, last accessed on 11 January 2023). For each fire, the database

provided the local coordinates; date and time; fire confidence; fire radiative power (expressed in megawatts); and type of hotspot (presumed vegetation fire, active volcano, other static land source, or offshore). For this study, we considered the FRP of all events with a fire confidence greater than 90% and classified as presumed vegetation fires.

2.6. Methods

For the 41 years of this study (1980–2020), a series of climatological fields were produced for each variable over the study region for the period spanning from June to September, hereafter referred to as the summer months. Climatologies for the whole year and for an extended period of colder months (November–April) may also be found in the Supplementary Material. Additionally, the intra-annual evolution of each index is presented in the form of boxplots, considering the clusters described in Section 2.1, where the box indicates the interquartile distance, the dash inside the box indicates the median, and the whiskers represent the 5th and 95th percentiles.

Changes in the CHI, FWI, and FWIe in the past four decades were assessed based on the seasonal variability, which was analyzed considering each decade independently. Additionally, we produced the same distributions for each cluster individually. Spatial change was assessed by computing the long-term trend for each of the variables using a monotonic seasonal Mann–Kendall trend test for the summer months. This trend is presented as the average index change per decade, and the non-significant areas (5% significance level) were identified.

The two fire risk indexes were compared with the observed FRPs over the IP, with the objective of comparing risk with occurrences. The FWI and FRP were stratified into predefined classes according to the following criteria: for FWI, the danger class system detailed in EFFIS [41], which presents the indexes in 6 classes ranging from “Very low” to “Extreme” danger; for the FRP, percentile-based classes as defined by percentiles 10, 33, 50, 67, and 90 of the FRP relative to the IP. For each of the FRP classes, a comparison was made between the FWI and FWIe associated with fire events. For this purpose, a linear regression was estimated for each FWI class (totaling 6 equations), the slope of each regression indicating which index had the largest magnitude. Furthermore, for each FRP class, a kernel density estimation (KDE) plot was obtained from the sample using a Gaussian kernel [42]. For both the linear regressions and the KDE plot, the FRP values were used as weights for the computations, i.e., the larger the FRP absolute value, the larger the influence on the result when comparing with other elements in the same set.

Furthermore, we also analyzed case studies: the two fire episodes of June and July 2017, and the two Monchique episodes of 2003 and 2018. The first case, in 2017, was chosen to validate the applied methodology by computing the indexes, as previous studies were available. The fire season of 2017 was exceptional for central and northern Portugal and parts of Galicia, although only the region inside the borders of Portugal and north of the 39.1° N parallel were analyzed in this study; this area encompassed 73% of all occurrences at that time and saw an excess burning of 500,000 ha and the tragic passing of 116 people [37]. Two additional case studies were conducted, wherein, instead of the whole fire season, only consecutive days of significant fires over a small area were analyzed. The fire season of 2003 was outstanding for western Europe and particularly for Portugal [6], with a massive fire that affected the Algarve, in the Monchique region. Years later, in 2018, 80% of this same region that had previously been affected was again subject to a large fire [43]. The choice of the study area in Monchique was motivated by the large mountain range in the area, increasing the interest regarding interactions with atmospheric instability. In all cases, a daily analysis was performed by taking the values of each variable and the respective daily FRP. Besides computing the absolute values of these variables, we also considered their anomalous character using standardized anomalies, i.e., the number of standard deviations above/below the climatological value for the region and the period. Additionally, we also computed the associated probability of exceedance assuming that the distribution of these values was normal.

3. Results

3.1. Climatological Analysis

In the summer months of JJAS, it was possible to identify higher CHI values in the southern part of Iberia, namely in the southeast/central east regions (Figure 2A), with a noticeable band at the 3° W meridian, which roughly corresponded to the junction of the Baetic Mountains, the Central System, and the Iberian System, all visible in the topographic map (Figure 1B). The spatial patterns of the FWI (Figure 2B) showed the largest values located over central Iberia, an area of a typical Mediterranean climate (Figure 1A), with hot to very hot and dry summers. Regions characterized by larger FWI values were typically contained inside the SW and E clusters. Finally, the spatial climatological pattern of the FWIe (Figure 2C) was overall more similar to that of the FWI, as was expected, since these variables were directly related. Nevertheless, the peak of CHI values observed in the border separating the SW and E clusters (Figure 2A) was partially recognizable in the FWIe (Figure 2C) but less evident in the original FWI pattern (Figure 2B). The spatial patterns of the CHI, FWI, and FWIe representing yearly and winter (DJF) climatologies may be found in Supplementary Materials Figure S1A–F, with similar results when considering the yearly patterns and noticeably lower values in winter.

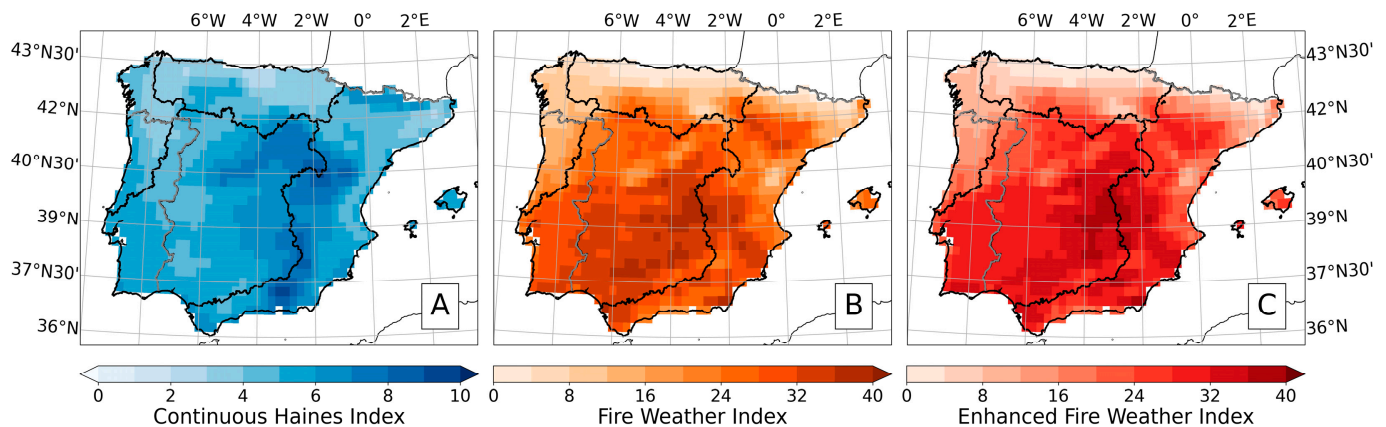


Figure 2. Field climatologies for the Iberian Peninsula for the 1980–2020 period considering the summer months of June, July, August, and September (JJAS) for the three indexes (A) CHI, (B) FWI, and (C) FWIe.

The annual cycle of the three indexes is displayed in the form of monthly boxplots in Figure 3 for each spatial cluster. The annual cycles depended on the region of analysis and were conditioned by the different types of climate, topography, and land cover, as depicted in Figure 1. The CHI distribution had the most notable change from region to region since the seasonal amplitude varied dramatically (Figure 3A–D). The northern part of Iberia, i.e., the NW and N clusters (Figure 3B,C, respectively), comprising the more humid areas of the Peninsula, showed lower overall CHI values (around 3 in winter and nearly 4 in the summer) and a lower yearly amplitude. In turn, the drier and warmer southern and central areas, i.e., the SW and E clusters (Figure 3A,D, respectively), showed the largest amplitude from winter to summer and the largest CHI values, surpassing 6. Additionally, the E cluster (Figure 3D) presented the greatest variability, namely in the warmer months. This higher variability found in the E cluster may have been due to the large meridional extent of the cluster, comprising regions from coastal to inland both in southern Spain and bordering the Pyrenees.

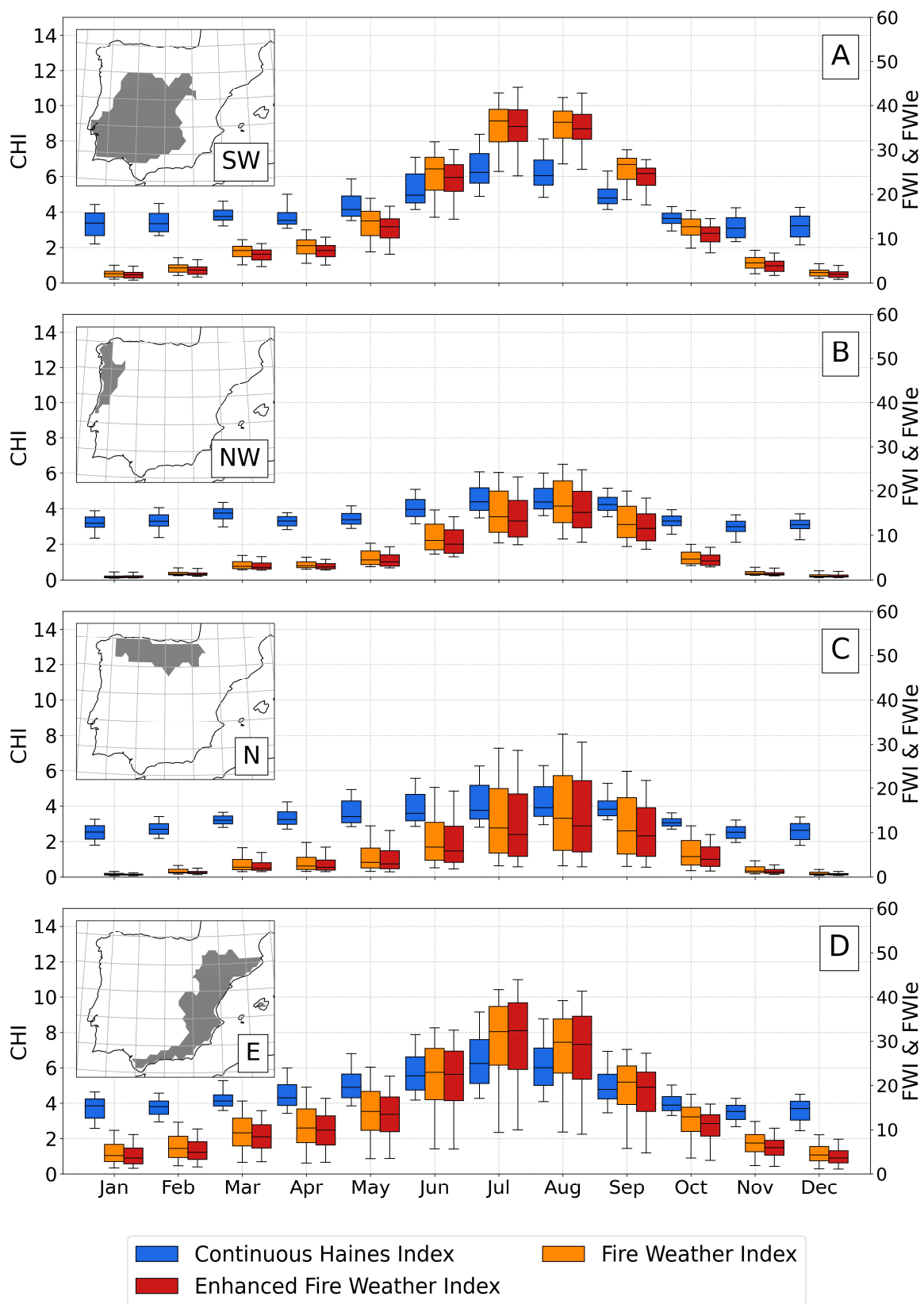


Figure 3. Annual cycles for each of the 4 clusters, (A) SW, (B) NW, (C) N and (D) E, during the period 1980–2020 for CHI (blue boxes), FWI (orange boxes), and FWIe (red boxes). The scale for CHI is on the left-hand y-axis, and the scale for FWI and FWIe is on the right-hand y-axis.

FWI, in comparison with CHI, had a more well-defined seasonality, with higher values and variability in the summer months (Figure 3A–D) and maximum median values around the 35 and 95th percentile maximums reaching 45. The SW cluster (Figure 3A) was characterized by a marked annual cycle in the FWI, with higher values in summer and low variability overall. Moreover, the variability of the FWI in the E region could be explained by its southernmost area sharing the characteristics of the SW cluster (higher FWI values in warmer months), while the northern area had a temperate oceanic climate (Figure 1A), with milder summers and winters (less seasonal temperature variation), contributing to a year-round lower FWI. The NW and N clusters (Figure 3B,C, respectively) had lower FWI scores when compared to the SW and E regions, with median values of 15 and 10, respectively. The NW region has a mostly warm summer Mediterranean climate, and the N region, with its mountainous character due to the presence of the Cantabrian Mountains (Figure 1B), has a mix of the above climate type and a temperate oceanic climate (Figure 1A). The annual cycles of the FWIe (Figure 3A–D) showed similar behavior to those of the FWI across all regions, usually with lower average and spread values, except for July and August in the E region (Figure 3D), where the variability increased overall. It is also noteworthy that different areas within these clusters presented different medians and respective extremes, due to the smaller-scale differences in land cover and climate types.

3.2. Decadal Evolution

Long-term changes were evaluated by performing a decadal evolution assessment of the IP average CHI, FWI, and FWIe values (Figure 4). From the decadal evolution of the CHI (Figure 4A), a similar seasonal cycle to that seen in Figure 3 may be noticed, with median values of around 3 in the colder months and exceeding 6 from June to August. Overall, the months of November, December, and January showed nearly no decadal changes, while from February to April there has been a slight decrease since the 1990s. However, from May to August we observed a general increase since the 1980s, which was also found for September and October since the 1990s (Figure 4A). We performed a similar assessment on a regional basis, and the main conclusions described above for the whole IP were also visible when considering the SW and E regions (Figure S2A and Figure S5A, respectively) and, to a lesser degree, the NW and N regions (Figure S3A and Figure S4A). The spatial distribution of long-term CHI trends is presented in Figure 5A, confirming the identified increments, with the greatest change in the CHI appearing to be mainly located in the southeastern region of the IP, presenting increases of approximately 0.25 and 0.26 per decade in the SW and E regions, respectively (Supplementary Material Table S1 fully describes the changes per decade and statistical significance). The NW and N regions showed smaller increases of about 0.06 and 0.15 per decade, respectively, with only 49% and 66% of their areas presenting statistically significant changes.

The decadal evolution of the IP average FWI and FWIe values (Figure 4B and Figure 4C, respectively) showed similar behaviors to those observed in the seasonal distributions of the SW and E regions (Figure 3A,D). As with the CHI, the colder months (in this case, from November to February) showed no substantial changes in either the FWI or FWIe, while in March and April there was a slight decrease after the 1990s. On the other hand, when considering the summer months, there was a general major increase, namely in May, July, and August. Conversely to the CHI, these increases affected all regions (Figures S2B–S5B and S2C–S5C), with special relevance in the SW and E regions. As with the CHI, the larger trends were located towards the southeast of the Peninsula (Figure 5B,C), with almost the entire IP presenting statistically significant positive trends. Figure 5C shows, for the FWIe, an extended region where the positive trends exceeded four per decade, which resulted from the combined increases in both the CHI and FWI around the same approximated areas. The SW and E regions showed the most relevant changes regarding these decadal trends, with the majority having significant grid boxes with large positive values. Of the SW region's territory, 100% presented statistical significance, and the region showed average increases of approximately 1.9 and 2.2 per decade for the FWI

and FWIe, respectively, while the E region showed slightly lower increases of circa 1.9 and 2.1 for the same variables (Table S1).

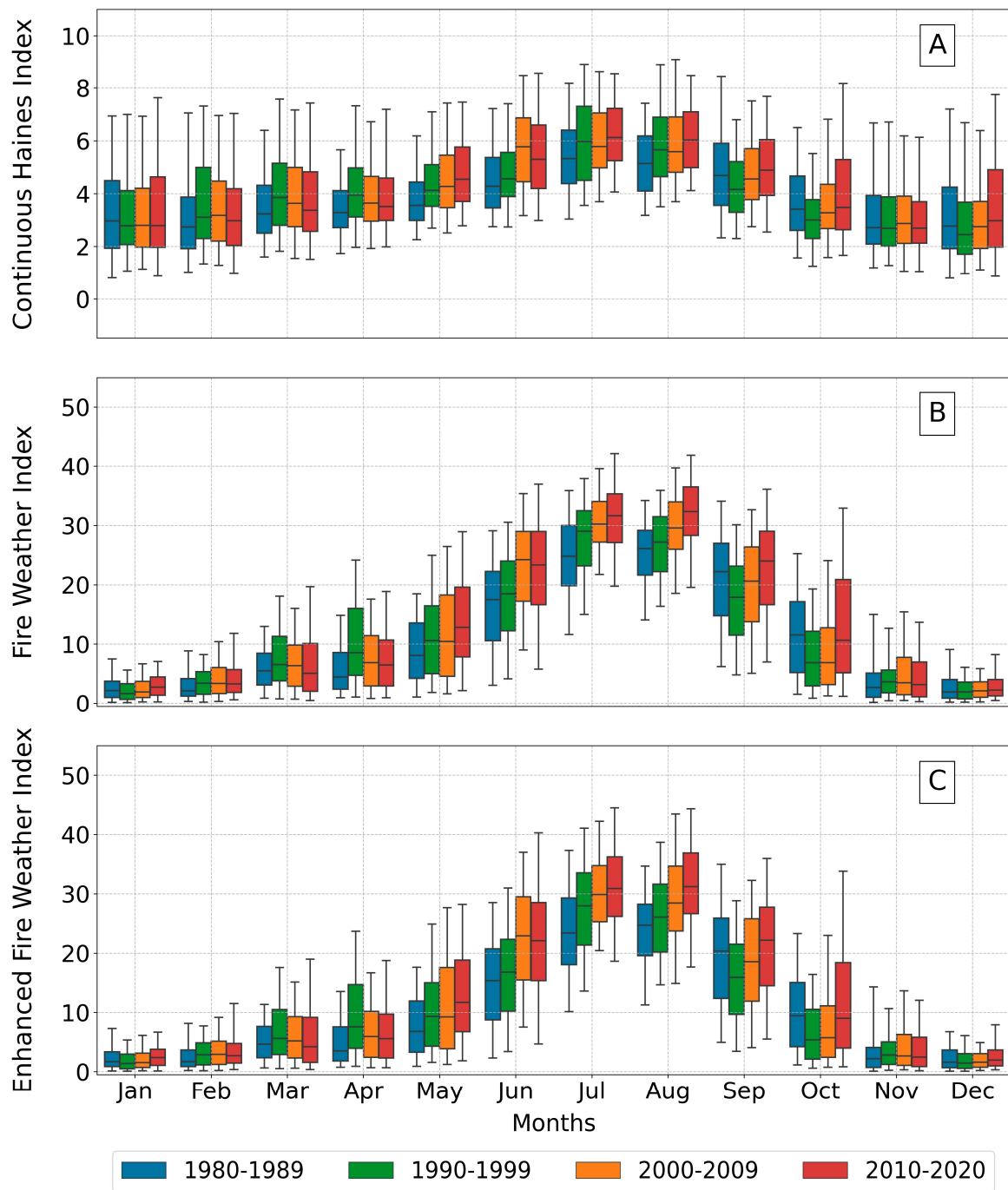


Figure 4. Boxplots showing evolution of the yearly distribution in the IP average throughout the decades of the 1980–2020 period for the variables (A) CHI, (B) FWI, and (C) FWIe.

3.3. Fire Occurrences and FWI vs. FWIe

The relationship with real fire occurrences was examined using FRP as a measure of the power released by each fire observation. We aggregated the computed FRP classes that were defined according to the values of the percentiles 10, 33, 50, 66, and 90 (respectively, 24.9, 53.6, 81.4, 130.1, and 362.3 MW). Each panel of Figure 6 presents the relationship between the FWI and FWIe in two different ways: (1) by means of KDE plots (as shown

by the grey scale) and (2) by means of linear regressions (as shown by the colored lines) estimated for each FWI class (shown as vertical black bars).

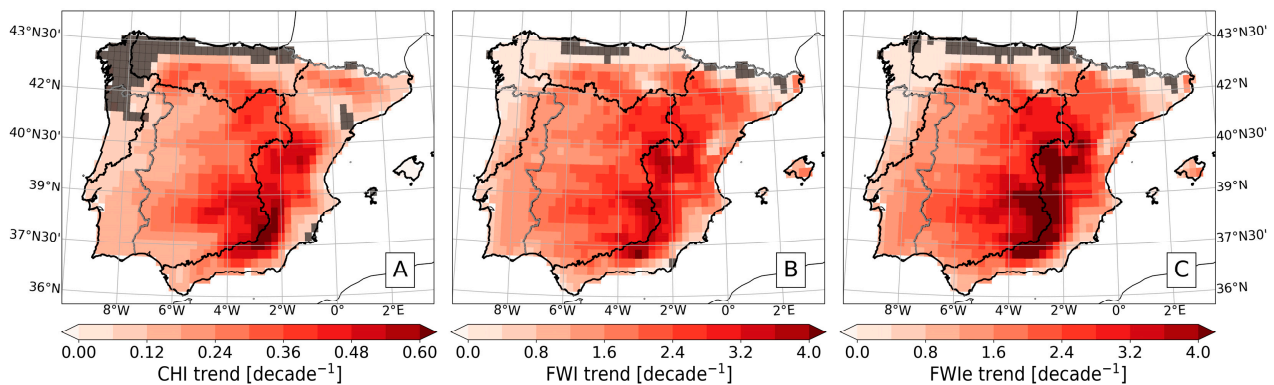


Figure 5. Long-term trends for (A) CHI, (B) FWI, and (C) FWIe, considering only summer months (June to September) for the 1980–2020 period. Computed from a monotonic seasonal Mann–Kendall trend test. Grey shaded areas show pixels where trends were not significant at the 5% statistical level. Trends are shown as the average index change per decade.

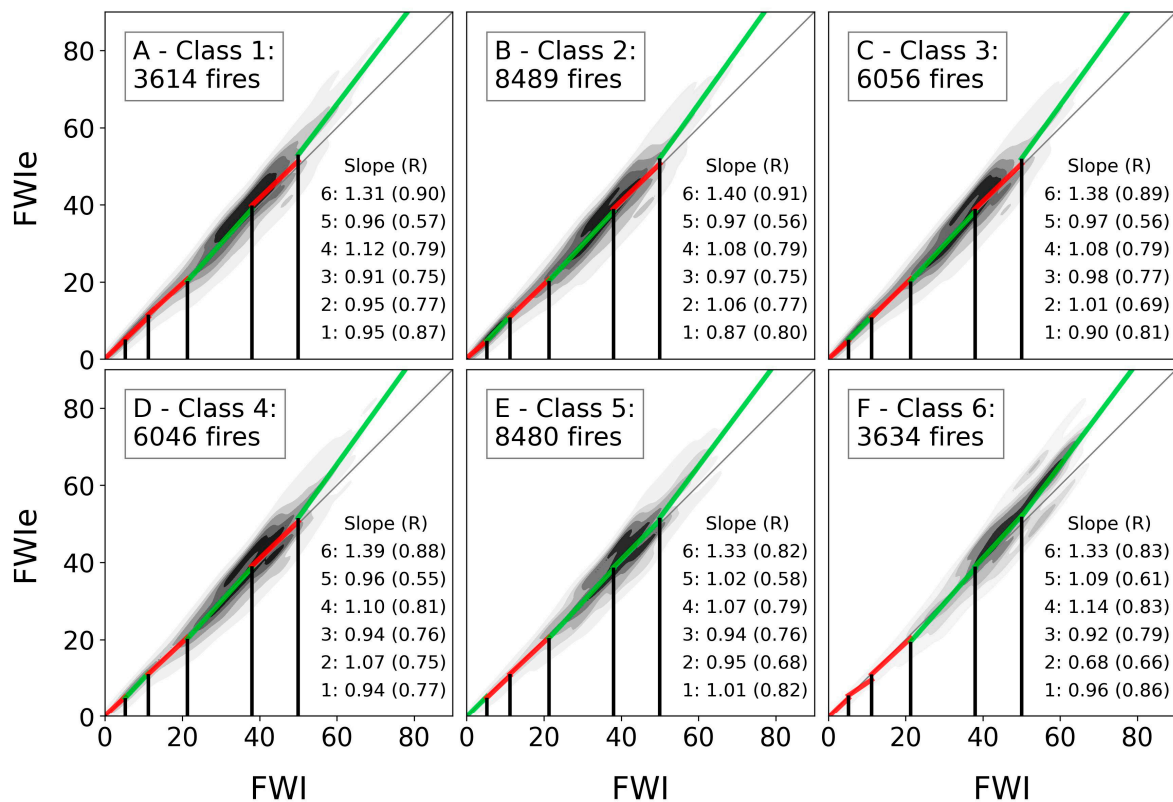


Figure 6. Comparison between real FRP observations (from 2001 to 2020, considering the whole IP) and the FWI and FWIe values for the same occurrences. Both FRP and fire danger indexes were divided into discrete divisions: FRP based on the percentiles 10, 33, 50, 67, and 90 of all occurrences (panels (A–F), with the respective number of FRPs in that division); and the FWI according to the fire danger classes provided by EFFIS (vertical black lines). The linear regressions for each FWI class compared to FWIe are shown by colored lines: red (green) for slope exceeding (subceeding) the identity line. Values of the slope and associated Pearson R values are shown in each panel, with ascending values (1–6) corresponding to the increasing FWI classes (bottom left to top right within each individual subplot).

It is immediately noticeable from the KDE plot that the bigger the occurrence (i.e., the higher the class of FRP), the more likely it was that an event would happen during more extreme values of the FWI. Fires with an FRP within the first four classes (Figure 6A–D), i.e., with an FRP lower than 130.1, were more likely to coincide with the “high danger” FWI class (up to the fourth vertical black line in Figure 6A–D), with upwards of 35% of these classes’ observations falling inside this FWI class. However, fires with FRPs larger than 130.1 corresponded to at most the “very high danger” FWI class (above the fourth vertical black line in Figure 6E,F), also having upwards of 35% representation in this class. It is worth noting that fires with the greatest FRP values (Figure 6F) happened more frequently during the “extreme” than the “high danger” FWI class (30% of the total number of the largest FRP occurrences compared to 25.3%), showing a complete shift in danger associated with the largest fires compared to small-FRP classes.

Looking closely at each FWI class for every panel (colored lines), the linear regression is presented with the associated slope (numerically and in color) and Pearson R value. The first notable detail when comparing the different panels is the FWI classes that preserved the slope type. Firstly, the middle FWI classes (“moderate” and “high”, third and fourth, respectively) showed the same behavior in all panels, with the “moderate” (“high”) class having a slope below (above) that of the identity line—averaging 0.94 (1.10)—meaning that the FWIe classified the same FRP with a lower (higher) value compared to the FWI. This behavior points to the different nature of the FWIe, which favored a higher danger index for higher FRP values in the upper middle classes. Adding to this, the “extreme” (sixth) FWI class consistently presented higher FWIe values, as seen in all FRP classes, with the highest R values being upwards of 0.83. The reverse could be verified in the “very low” (first) FWI class, with the exception of the fifth (Figure 6E) FRP class. Additionally, the “very high” (fifth) FWI class presented slopes below the identity line in the first four FRP classes (Figure 6A–D), while the last two were above the line (Figure 6E,F); thus, higher (lower) FRP observations were better represented by higher FWIe (FWI) values. To conclude, Figure 6 shows that, overall, higher-FRP occurrences (i.e., more intense fires) tended to logically occur under higher FWI values, and the FWIe generally increased the meteorological danger for these occurrences, while in lower FWI classes, this index maintained greater values compared to the FWIe.

3.4. Case Studies

Figure 7 aggregates the information regarding the CHI, FWI, FWIe, and FRP during the 2017 extended fire season in Portugal, as well as the shapes of all identified burned areas. For the first episode, on June 17th, the CHI reached a value of nearly 10, an extreme value with a probability of exceedance of around 2.5%. This propelled the increase in the FWIe with respect to the FWI, with the latter having a value exceeding 30 and the former reaching 40, which was close to the 2.5% probability of exceedance (Figure 7B). This episode, as evidenced by the grey bars (representing the natural logarithm of the FRP) in Figure 7A, had one of the highest FRP values of this fire season, while the affected area was quite large, as evidenced by Figure 7C (in red). The October 15th episode, towards the end of the extended fire season, showed the maximum recorded FWI values for this region, with a probability of exceedance in the order of 0.005% (Figure 7B). During this episode, as already mentioned, the CHI was also very high, with values resembling those of June (~10, with a probability of exceedance of 2.5%); however, in this instance, the increment observed in the FWIe with respect to the FWI was not so relevant, since the latter was already a record value in itself. This episode led to by far the largest burned area, as seen in Figure 7C (in purple), with several major scars (several larger than 20,000 ha) located all over central and northern Portugal. Comparing both episodes, it became apparent that the June event was more strongly influenced by atmospheric instability, as mentioned in Pinto et al. [37] and depicted in Figure 7, while this contribution was lower in the October episode. These results reinforced the idea that considering the atmospheric instability as

well as the associated meteorological fire danger can provide more insightful information to better characterize extreme events.

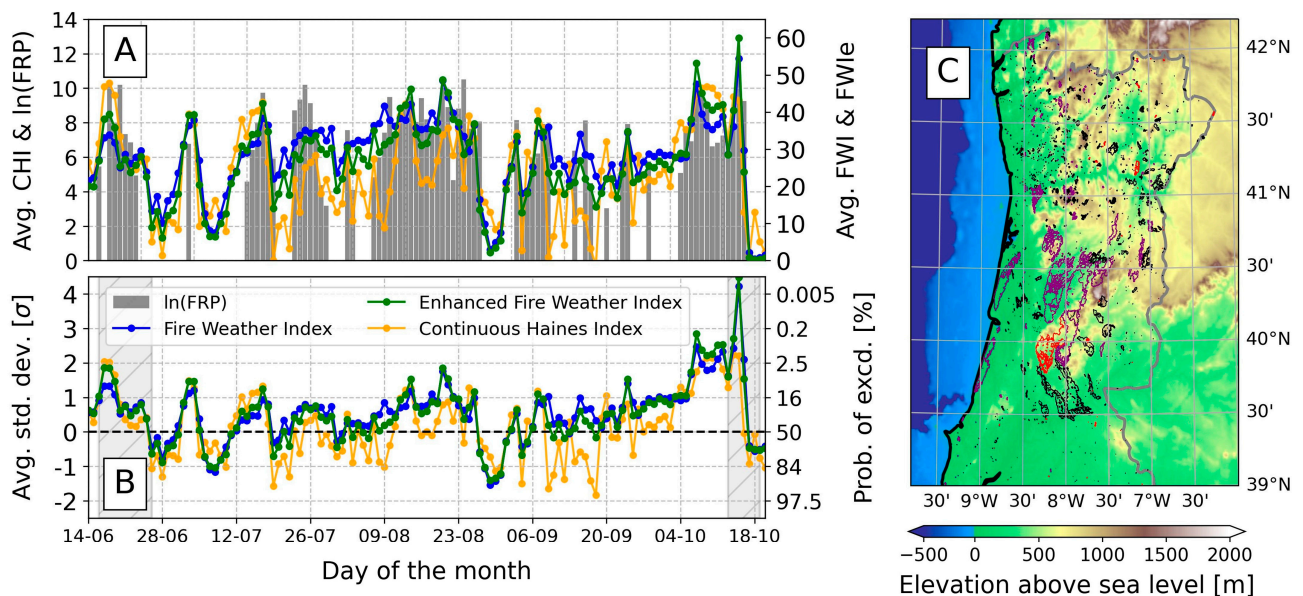


Figure 7. Comparison of the evolution of the CHI (yellow), FWI (blue), and the resulting FWIe (green) during the Portuguese 2017 fire season. (A) shows the daily average of each variable spatially averaged over the affected areas in Portugal and the natural logarithm of the daily FRP sum in grey bars. (B) shows the exceedance over (or under) the mean value of each variable in the number of standard deviations, and the approximate probability of exceedance can be seen on the right. Shaded grey areas represent the two time periods of the case studies mentioned above and are shown in (C) with the respective affected areas in different colors (red for 16–25 June and purple for 13–18 October). More details can be found in the Methods subsection.

The two Monchique study cases considered here are shown in Figure 8. In the top panel (Figure 8A), the location of these events in the southwestern IP region of Algarve, Portugal, is presented. The two-colored outlines denote the two burned areas for 2003 (the larger shape, in purple) and 2018 (the smaller shape, in red). Additionally, the topography of the area, which is presented as a color map, shows that the affected region was mostly mountainous, topping out at roughly 900 m but with several peaks reaching 600 m. This area mostly features a warm summer Mediterranean climate, generally with mild wet winters (Figure 1A), and has a land cover composed mostly of shrubs and forest (Figure 1C). The middle and bottom panels (Figure 8(B1–B3,C1–C3)) show the cases for August 2003 and August 2018, respectively, including the absolute values, the associated excess standard deviation, and the probability of exceedance for all indexes. However, these cases only show the period corresponding to the large fires in the region, depicted in Figure 8(B3,C3) as both the individual FRP observations (scattered dots colored according to the time of occurrence) and the burned area captured in later reports (grey shading; Figure 8(B3) contains regions with no FRP shown inside the shape, since the event occurred later in the season).

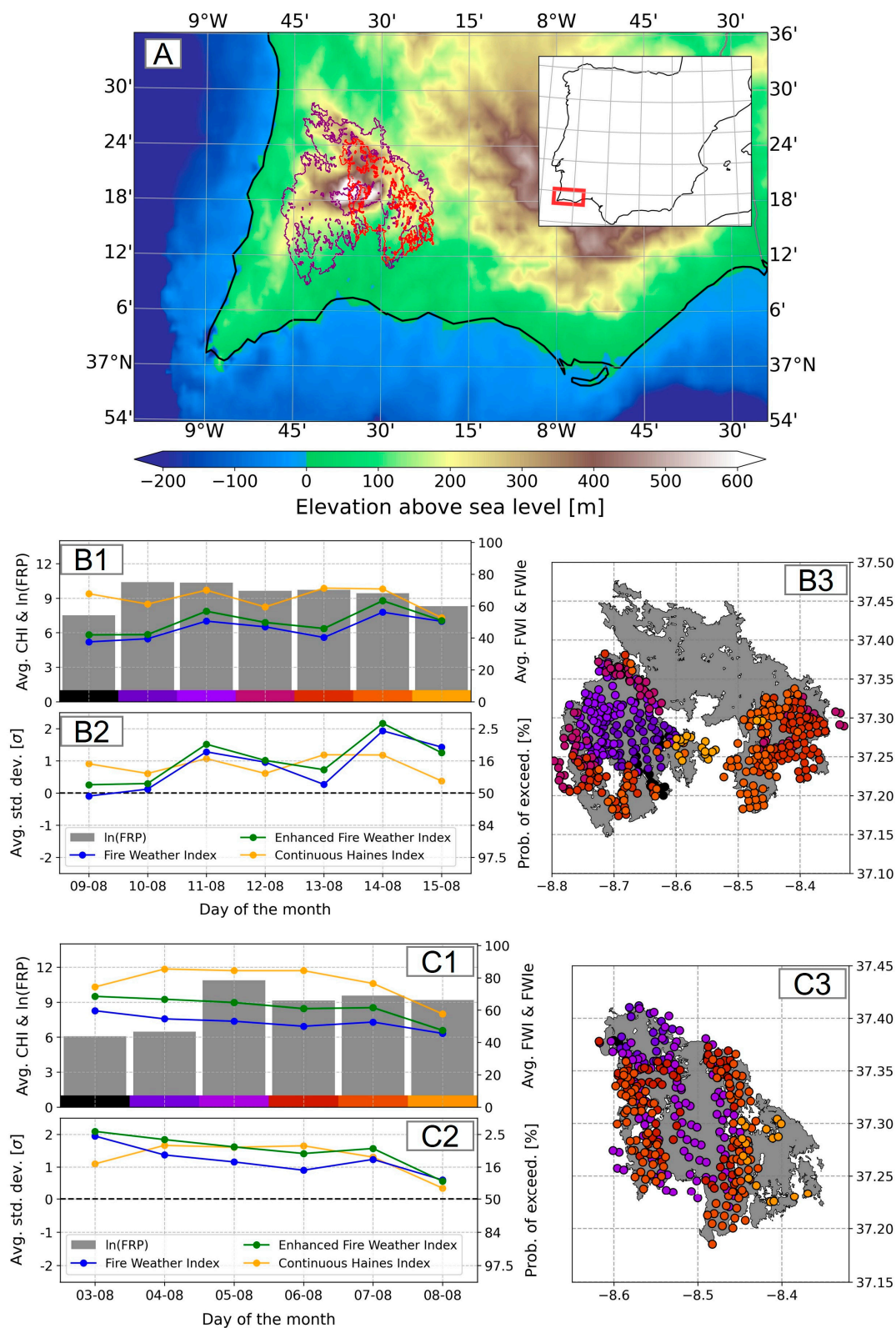


Figure 8. Study case for the Monchique region. Panel (A) shows the analyzed area, with the shapes representing the burned areas for 2003 (purple) and 2018 (red); topography is shown by colors. Panels (B1–B3) and (C1–C3) show the respective episodes for 2003 and 2018. Subplots 1 and 2 in these panels are as shown in Figure 6, with the addition of the colors corresponding to the day in subplot 3, depicting the affected region and the FRP location via the scattered colored dots.

The August 2003 Monchique study case (Figure 8(B1–B3)) actually comprised two distinct events that occurred close together in time and space. Starting on the 9th of August in the center-right area of the burned shape (Figure 8(B3)), the FWI values were not persistently high on this day over this region, reaching about 38 (Figure 8(B1)) and being close to the mean value (Figure 8(B2)). Atmospheric instability, however, was high, with CHI values above 9 (Figure 8(B1)), nearly one standard deviation above the mean value for this region at this time (Figure 8(B2)). These high CHI values clearly influenced the FWIe to be higher than the FWI; therefore, at this time, the atmospheric instability played a substantial role in increasing the meteorological fire danger FWIe associated with the beginning of this event. As it evolved over the next two days, the FWI increased greatly, while the CHI remained essentially unchanged. During these days, the greatest FRPs were registered (grey bars in Figure 8(B1); note the logarithmic scale), as most of the burned area in Figure 8(B3) was affected. From the 13th of August onwards, a secondary event evolved, eastward of the first one (right side of Figure 8(B3)). At first, the FWI values fell substantially with respect to the previous days, while the CHI was still high, thus increasing the FWIe (Figure 8(B1,B2))—a near copy of the situation on the 9th of August. The following day, the FWI increased to the highest values in this case study, and, with the aid of the still high CHI, the FWIe neared 60, exceeding the two standard deviations over the mean value for this region at that time, with a probability of exceedance below 2.5% (Figure 8(B1,B2)). The last day saw a decrease in the CHI, thus inducing a larger reduction in the FWIe to values identical to those of the FWI, although they were still high; this day coincided with the last FRP observations for this event.

The last study referred to the event that occurred in August 2018, mostly over the area that had already been affected in 2003, as seen in Figure 8A. This case was marked by a high fire meteorological danger, and high FRP values were initially captured on the 3rd of August, with FWI values above 50, which was two standard deviations above the mean value for this region, and a probability of exceedance close to 2.5% (Figure 8(C1,C2)). At the beginning, the CHI was high, with values approaching 11; however, the difference was not substantial between the FWI and FWIe (Figure 8(C1,C2))—similar behavior to that for October 2017 depicted in Figure 7. As the days progressed, the FWI decreased while the CHI increased to more exceptional values (near 12), causing the decrease in the FWIe to be slightly less substantial, and during these days (more specifically, on the 5th of August) the largest FRPs were registered. The last two days of this event saw a decrease in the atmospheric instability, which resulted in the FWIe values approaching those of the FWI.

4. Discussion and Summary

This study comprehensively analyzed the relationship between atmospheric instability and fire risk using the novel FWIe, recently developed by Pinto et al. [18], which associates the well-established instability index known as the Continuous Haines Index (CHI) and the most widely used meteorological fire danger index, the FWI. We extensively studied this relationship over the IP from a climatological viewpoint for the period of 1980 to 2020. Additionally, we considered the observed occurrences of fires according to the FRP from 2001 to 2020 and compared them to several fire danger classes proposed by EFFIS. Finally, we examined several specific case studies to identify the behavior of the new FWIe in relation to the older FWI and checked its success in assessing meteorological fire danger over the Iberian region.

A climatological analysis of the CHI showed that the largest values of this atmospheric instability metric were located mainly in the southern region of Iberia. This may be attributed to the more complex topography of the region—although the northern part of Iberia presents some complex topography, the temperatures are substantially lower, de-creasing the convective instability [44]. The regions that correspond to the junction of the Baetic Mountains, the Central System, and the Iberian System presented the largest values of the CHI in summer, with an absolute maximum in Sierra Nevada. Regarding the FWI and FWIe, the highest values were found in southern regions, which are not

typically fire-prone locations. Indeed, the land cover over these areas is mainly cropland, and the only vegetated areas are in mountainous regions. The most fire-prone regions were those located in northwestern Iberia, namely the north of Portugal and the Spanish northwest region of Galicia [45], which, although showing lower values of the FWI and FWIe, must be considered as critical regions due to a combination of weather/climate, vegetation, geographical, and human factors [33]. Furthermore, the northwestern IP is also a crucial region of rising fire danger for the future, especially in the months of June, July, and August [9]. The values of the FWIe tended to be on average lower than those of the FWI, implying that predominantly stable conditions decreased (albeit slightly) the fire risk level provided by the standard FWI. This may be viewed as an inherent characteristic of the new enhanced FWIe, which favored an increase in the more extreme values to better evaluate the most intense occurrences and downgraded the less dangerous ones [18].

In addition to their seasonal variability, the three indexes significantly increased over the past four decades. These increases were prevalent over the warmer months from May to October, especially affecting the meteorological fire danger indexes (FWI and FWIe), which had major increases in May, July, and August, months belonging to the so-called extended fire season. During these warmer months, most of the IP suffered a significant increase in all three variables, with the exception of the northwestern part of Iberia in the NW and N clusters for the CHI. The SW and E regions were again found to be characterized by the most significant increments in long-term trends. The maximum decadal trends of the FWIe occupied a much larger area compared to those of the FWI; this was expected, since the FWIe incorporated results from the CHI and FWI, which did not present maximum decadal trends that coincided spatially. The specific location of these changes should be further analyzed in future studies focused on local-scale analysis. Moreover, several studies have predicted an increase in fire-danger-associated indexes, namely the FWI, associated with an increase in the mean air temperature in most of this region, related to anthropogenic climate change [1,7–9,32].

Comparing the FWI and FWIe, we found the latter to be useful in differentiating events in which convective meteorological situations helped to enhance the fire risk and eventually fire propagation. This was determined by considering different classes of observed fire occurrences (in the form of FRP values) and comparing these to the fire danger classes proposed by EFFIS. The comparison between the observed FRPs and the calculated FWI and FWIe values allowed us to verify that the higher the FRP class (i.e., the larger the occurrence), the greater the probability of the observations falling into the higher FWI classes. In fact, in the two strongest FRP classes (i.e., above 130.1 MW), the biggest FWI classes (i.e., “high” danger and upwards) presented consistently higher FWIe compared to FWI values. These results led to the conclusion that the FWIe better represented the meteorological fire danger in these extreme cases. Overall, our results showed that higher FRP classes were more prone to be affected by atmospheric instability than lower meteorological fire danger situations. Moreover, for most of the six FRP classes considered, the reverse was also found (despite some marginal exceptions), with lower danger classes (i.e., “moderate” danger and below) presenting a higher FWI compared to FWIe value. To conclude, we can state that higher FRP values (i.e., more intense fires) tended to occur in concert with higher FWI values, and the FWIe generally increased the meteorological danger for these occurrences; conversely, for lower FWI classes, this index maintained greater values compared to the FWIe.

The two case studies of the 2017 Portuguese fire season, which took place on the 17th of June and on the 15th of October, were thoroughly compared [37]. The results showed that the June episode presented larger convective circulation, which helped to propel the fire intensity, i.e., the CHI was higher, and therefore the fire risk was much higher. On the other hand, the October episode included the aggravating passage of Hurricane Ophelia (2017) just west of the Iberian coast, which, despite not directly increasing the convective circulation over the region, increased the wind intensities observed in these areas, which in turn induced increased CHI values. Overall, despite their very different nature and impacts, both extreme fire episodes in 2017 included a high convective potential for fire

spreading, although this mechanism was more relevant for the June episodes according to [37].

Finally, we evaluated the role of the CHI, FWI, and FWIe for the case studies of the Monchique megafires that occurred in the 2003 and 2018 fire seasons in southwestern IP. The 2003 event covered two August fires, the first started on the 8th at Marmeleite and the second initiated on the 12th at Silves. At the beginning of both occurrences, atmospheric instability was found to be significant in enhancing the meteorological fire danger in the form of the FWIe, while at the very end of the episodes the reverse was observed, and the value of the FWIe fell below that of the FWI. In 2018, the event also took place in August, starting on the 3rd near the town of Monchique; 80% of the area affected by this fire had already been burned by the previous fires from 2003. In this case, the FWI presented high values throughout the event, though with a small decrease and high atmospheric instability at the beginning. As the event progressed, the instability increased, attenuating the decrease observed in the FWI during the days with the greatest FRPs. At the end of the event, both the instability and the meteorological fire danger decreased substantially, encouraging the end of the event. These case studies both affected the same general area (the slopes of the Monchique Range), 15 years apart. As previously mentioned, the CHI was observed to be higher in places of topographic complexity, and, as these case studies made clear, the atmospheric instability (that was already high in these places) showed exceptional values above 10 (reaching 12 in 2018). Previous studies have pointed out that extreme CHI values above 10 imply that it is extremely complex to extinguish fires, and there is an aggravated risk of under-predicted fire behavior [29]. These facts combined indicate that atmospheric instability played an important role in both events.

5. Final Remarks

This study was performed in the framework of the National Roadmap for Adaptation XXI—Portuguese Territorial Climate Change Vulnerability Assessment for XXI Century (RNA2100) project, which is currently being developed with the aim of supporting public policy exercises related to adaptation to climate change. This work aimed to contribute to the development and assessment of a state-of-the-art meteorological fire risk index, the FWIe, which was designed to improve the traditional FWI by incorporating explicitly in its formulation the role played by atmospheric instability. This new enhanced index may represent an important tool, contributing to the forest and wildfire sector's decision-makers, since atmospheric instability is known to play a crucial role in the development of some large wildfires. Indeed, this was the case in the deadly wildfires that occurred in Portugal in June 2017, as shown by the case study analyzed in this paper. Additionally, from a more structural perspective, this work aimed at assessing the FWIe using reanalyzed ERA5 data and paves the way for the development of storylines focused on destructive wildfire events in a climate change context, contributing to the development of timely adaptation strategies. This work overall highlighted the great importance of atmospheric instability in the development of extreme-fire-risk events, providing essential evidence to improve early warning systems in certain places to prevent large catastrophes from happening, such as the increased effectiveness of the FWIe to predict more or less extreme danger situations compared to the more well-established FWI. Future developments in this area are therefore recommended, both locally, regarding potential links with land cover and geographical features such as river basins, near-shore locations, or mountainous areas, and on a policy level, with better territorial planning and vegetation management.

Supplementary Materials: The following supporting information can be downloaded at: <https://www.mdpi.com/article/10.3390/fire6030120/s1>, Figure S1: Yearly and winter field climatology for the Iberian Peninsula, Figure S2: Decadal evolution of the yearly distribution in the SW cluster for the three variables CHI (A), FWI (B), and FWIe (C), Figure S3: Same as Figure S2 but for the NW cluster, Figure S4: Same as Figure S2 but for the N cluster, Figure S5: Same as Figure S2 but for the E cluster, Table S1: Average geographical trend in each cluster for all three variables.

Author Contributions: L.C.S. and M.M.L.: conceptualization; methodology; software; validation; formal analysis; investigation; data curation; writing (original draft preparation, review, and editing); and visualization. V.A.B. and S.A.N.: validation, formal analysis, investigation, data curation, writing (review and editing), and supervision. C.C.D., A.R., P.M.M.S. and R.M.T.: validation, writing (review and editing), and supervision. R.M.T.: project administration. All authors have read and agreed to the published version of the manuscript.

Funding: This work was funded by EEA-Financial Mechanism 2014–2021 and the Portuguese Environment Agency through Pre-defined Project-2 National Roadmap for Adaptation XXI (PDP-2) and the project “Forecasting fire probability and characteristic for a habitable pyro environment (Fire-Cast)” under grant no. PCIF/GRF/0204/2017, and by the Portuguese Fundação para a Ciência e a Tecnologia (FCT) I.P./MCTES through national funds (PIDDAC)—UIDB/50019/2020.

Institutional Review Board Statement: Not applicable.

Informed Consent Statement: Not applicable.

Data Availability Statement: ERA5 hourly data may be found at <https://www.ecmwf.int/en/forecasts/datasets/reanalysis-datasets/era5>, last accessed on 11 January 2023. Corine Land Cover was retrieved from <https://land.copernicus.eu/>, last accessed on 11 January 2023. MODIS FRP was downloaded from <https://earthdata.nasa.gov>, last accessed on 11 January 2023. Burned area scars were extracted from <https://www.icnf.pt/>, last accessed on 11 January 2023. All the code used to process the data is available upon request without undue reservation.

Acknowledgments: L.C.S. would like to acknowledge the financial support of FCT through the project “Forecasting fire probability and characteristics for a habitable pyroenvironment (Fire-Cast)” under grant no. PCIF/GRF/0204/2017. M.M.L. would like to acknowledge the project “Extração de dados por chamada de url com parâmetros—CEASEFIRE”, financed by E-REDES. V.A.B. is funded by the Pre-defined Project-2 National Roadmap for Adaptation XXI (PDP-2).

Conflicts of Interest: The authors declare no conflict of interest.

References

1. Amatulli, G.; Camia, A.; San-Miguel-Ayanz, J. Estimating future burned areas under changing climate in the EU-Mediterranean countries. *Sci. Total Environ.* **2013**, *450*, 209–222. [[CrossRef](#)] [[PubMed](#)]
2. Amraoui, M.; Pereira, M.G.; DaCamara, C.C.; Calado, T.J. Atmospheric conditions associated with extreme fire activity in the Western Mediterranean region. *Sci. Total Environ.* **2015**, *524*, 32–39. [[CrossRef](#)] [[PubMed](#)]
3. Fernandes, P.M.; Monteiro-Henriques, T.; Guiomar, N.; Loureiro, C.; Barros, A.M. Bottom-up variables govern large-fire size in Portugal. *Ecosystems* **2016**, *19*, 1362–1375. [[CrossRef](#)]
4. Carmo, M.; Ferreira, J.; Mendes, M.; Silva, Á.; Silva, P.; Alves, D.; Reis, L.; Novo, I.; Viegas, D.X. The climatology of extreme wildfires in Portugal, 1980–2018: Contributions to forecasting and preparedness. *Int. J. Climatol.* **2021**, *42*, 3123–3146. [[CrossRef](#)]
5. DaCamara, C.C.; Calado, T.J.; Ermida, S.L.; Trigo, I.F.; Amraoui, M.; Turkman, K.F. Calibration of the fire weather index over mediterranean europe based on fire activity retrieved from msg satellite imagery. *Int. J. Wildland Fire* **2014**, *23*, 945–958. [[CrossRef](#)]
6. Trigo, R.M.; Pereira, J.M.; Pereira, M.G.; Mota, B.; Calado, T.J.; Dacamara, C.C.; Santo, F.E. Atmospheric conditions associated with the exceptional fire season of 2003 in Portugal. *Int. J. Climatol.* **2006**, *26*, 1741–1757. [[CrossRef](#)]
7. Abatzoglou, J.T.; Williams, A.P.; Barbero, R. Global emergence of anthropogenic climate change in fire weather indices. *Geophys. Res. Lett.* **2019**, *46*, 326–336. [[CrossRef](#)]
8. Bedia, J.; Herrera, S.; Camia, A.; Moreno, J.M.; Gutiérrez, J.M. Forest fire danger projections in the Mediterranean using ENSEMBLES regional climate change scenarios. *Clim. Change* **2014**, *122*, 185–199. [[CrossRef](#)]
9. Calheiros, T.; Nunes, J.P.; Pereira, M.G. Recent evolution of spatial and temporal patterns of burnt areas and fire weather risk in the Iberian Peninsula. *Agric. Forest Meteorol.* **2020**, *287*, 107923. [[CrossRef](#)]
10. Pereira, M.G.; Calado, T.J.; DaCamara, C.C.; Calheiros, T. Effects of regional climate change on rural fires in Portugal. *Clim. Res.* **2013**, *57*, 187–200. [[CrossRef](#)]
11. Lionello, P.; Malanotte-Rizzoli, P.; Boscolo, R.; Alpert, P.; Artale, V.; Li, L.; Luterbacher, J.; May, W.; Trigo, R.; Tsimplis, M.; et al. The Mediterranean climate: An overview of the main characteristics and issues. *Dev. Earth Environ. Sci.* **2006**, *4*, 1–26. [[CrossRef](#)]
12. Nunes, S.A.; DaCamara, C.C.; Turkman, K.F.; Calado, T.J.; Trigo, R.M.; Turkman, M.A. Wildland fire potential outlooks for Portugal using meteorological indices of fire danger. *Nat. Hazard. Earth Sys.* **2019**, *19*, 1459–1470. [[CrossRef](#)]
13. San-Miguel-Ayanz, J.; Durrant, T.; Boca, R.; Maianti, P.; Libertá, G.; Artés Vivancos, T.; Jacome Felix Oom, D.; Branco, A.; De Rigo, D.; Ferrari, D.; et al. *Forest Fires in Europe, Middle East and North Africa 2020*; Publications Office of the European Union: Luxembourg, 2021. [[CrossRef](#)]

14. Leone, V.; Lovreglio, R.; Martín, M.P.; Martínez, J.; Vilar, L. Human factors of fire occurrence in the Mediterranean. In *Earth Observation of Wildland Fires in Mediterranean Ecosystems*, 1st ed.; Springer: Berlin, Germany, 2009; pp. 149–170. [[CrossRef](#)]
15. Gómez-González, S.; Ojeda, F.; Fernandes, P.M. Portugal and Chile: Longing for sustainable forestry while rising from the ashes. *Environ. Sci. Policy* **2018**, *81*, 104–107. [[CrossRef](#)]
16. Alcubierre, P.C.; Ribau, M.C.; de Egileor, A.L.O.; Bover, M.M.; Kraus, P.D. *Prevention of Large Wildfires Using the Fire Types Concept*; Unitat Técnica del GRAF: Barcelona, Spain, 2011.
17. Lecina-Diaz, J.; Alvarez, A.; Retana, J. Extreme fire severity patterns in topographic, convective and wind-driven historical wildfires of Mediterranean pine forests. *PLoS ONE* **2014**, *9*, e85127. [[CrossRef](#)] [[PubMed](#)]
18. Pinto, M.M.; DaCamara, C.C.; Hurduduc, A.; Trigo, R.M.; Trigo, I.F. Enhancing the fire weather index with atmospheric instability information. *Environ. Res. Lett.* **2020**, *15*, 0940b7. [[CrossRef](#)]
19. Ruffault, J.; Moron, V.; Trigo, R.M.; Curt, T. Daily synoptic conditions associated with large fire occurrence in Mediterranean France: Evidence for a wind-driven fire regime. *Int. J. Climatol.* **2017**, *37*, 524–533. [[CrossRef](#)]
20. Flatley, W.T.; Lafon, C.W.; Grissino-Mayer, H.D. Climatic and topographic controls on patterns of fire in the southern and central Appalachian Mountains, USA. *Landsc. Ecol.* **2011**, *26*, 195–209. [[CrossRef](#)]
21. Lareau, N.P.; Clements, C.B. The mean and turbulent properties of a wildfire convective plume. *J. Appl. Meteorol. Clim.* **2017**, *56*, 2289–2299. [[CrossRef](#)]
22. Jolly, W.M.; Freeborn, P.H.; Page, W.G.; Butler, B.W. Severe fire danger index: A forecastable metric to inform firefighter and community wildfire risk management. *Fire J.* **2019**, *2*, 47. [[CrossRef](#)]
23. Van Wagner, C. *Development and Structure of the Canadian Forest Fire Weather Index System*; Can. For. Serv., Forestry Tech. Rep.: Ottawa, Canada, 1987.
24. Karali, A.; Roussos, A.; Giannakopoulos, C.; Hatzaki, M.; Xanthopoulos, G.; Kaoukis, K. Evaluation of the Canadian Fire Weather Index in Greece and future climate projections. In *Advances in Meteorology*; Springer: Berlin/Heidelberg, Germany, 2013; pp. 501–508. [[CrossRef](#)]
25. Pinto, M.M.; DaCamara, C.C.; Trigo, I.F.; Trigo, R.M.; Turkman, K.F. Fire danger rating over mediterranean europe based on fire radiative power derived from meteosat. *Nat. Hazard Earth Sys.* **2018**, *18*, 515–529. [[CrossRef](#)]
26. Wang, Y.; Anderson, K.R.; Suddaby, R.M. Updated source code for calculating fire danger indices in the Canadian Forest Fire Weather Index System. In *Canadian Forest Service, Northern Forestry Centre Information Rep, Natural Resources Canada*; NOR-X-424: Edmonton, Canada, 2015; p. 26. Available online: <https://cfs.nrcan.gc.ca/publications> (accessed on 11 March 2022).
27. Haines, D.A. A lower atmospheric severity index for wildland fires. *Natl. Weather. Dig.* **1988**, *13*, 23–27.
28. Dowdy, A.J.; Pepler, A. Pyroconvection risk in Australia: Climatological changes in atmospheric stability and surface fire weather conditions. *Geophys. Res. Lett.* **2018**, *45*, 2005–2013. [[CrossRef](#)]
29. Mills, G.A.; McCaw, L. *Atmospheric Stability Environments and Fire Weather in Australia—Extending the Haines Index*; Technical Report; Centre for Australian Weather and Climate Research: Victoria, Australia, 2010; Volume 20.
30. Stull, R.B. *An Introduction to Boundary Layer Meteorology*; Springer: Berlin/Heidelberg, Germany, 1988; Volume 13.
31. Hersbach, H.; Bell, B.; Berrisford, P.; Hirahara, S.; Horányi, A.; Muñoz-Sabater, J.; Nicolas, J.; Peubey, C.; Radu, R.; Schepers, D.; et al. The era5 global reanalysis. *Q. J. R. Meteor. Soc.* **2020**, *146*, 1999–2049. [[CrossRef](#)]
32. Sousa, P.M.; Trigo, R.M.; Pereira, M.G.; Bedia, J.; Gutiérrez, J.M. Different approaches to model future burnt area in the Iberian Peninsula. *Agric. Forest Meteorol.* **2015**, *202*, 11–25. [[CrossRef](#)]
33. Trigo, R.M.; Sousa, P.M.; Pereira, M.G.; Rasilla, D.; Gouveia, C.M. Modelling wildfire activity in Iberia with different atmospheric circulation weather types. *Int. J. Climatol.* **2016**, *36*, 2761–2778. [[CrossRef](#)]
34. Chen, D.; Chen, H.W. Using the Köppen classification to quantify climate variation and change: An example for 1901–2010. *Environ. Dev.* **2013**, *6*, 69–79. [[CrossRef](#)]
35. Smith, W.H.; Sandwell, D.T. Global sea floor topography from satellite altimetry and ship depth soundings. *Science* **1997**, *277*, 1956–1962. [[CrossRef](#)]
36. Büttner, G.; Kosztra, B.; Kleeschulte, S.; Hazeu, G.; Vittek, M.; Schroder, C.; Littkopf, A. *Copernicus Land Monitoring Service: Corine Land Cover*; EEA: Copenhagen, Denmark, 2021.
37. Pinto, M.M.; Hurduduc, A.; Trigo, R.M.; Trigo, I.F.; DaCamara, C.C. The extreme weather conditions behind the destructive fires of June and October 2017 in Portugal. In *Advances in Forest Fire Research*; University of Coimbra: Coimbra, Portugal, 2018. [[CrossRef](#)]
38. Winkler, J.A.; Potter, B.E.; Wilhelm, D.F.; Shadbolt, R.P.; Piromsopa, K.; Bian, X. Climatological and statistical characteristics of the Haines Index for North America. *Int. J. Wildland Fire* **2007**, *16*, 139–152. [[CrossRef](#)]
39. Lawrence, M.G. The relationship between relative humidity and the dewpoint temperature in moist air: A simple conversion and applications. *B. Am. Meteorol. Soc.* **2005**, *86*, 225–234. [[CrossRef](#)]
40. Giglio, L.; Schroeder, W.; Hall, J.V.; Justice, C.O. *MODIS Collection 6 Active Fire Product User's Guide Revision B*; Department of Geographical Sciences, University of Maryland: College Park, MD, USA, 2018.
41. European Forest Fire Information System (EFFIS). “Fire Danger Forecast”. Available online: <https://effis.jrc.ec.europa.eu/about-effis/technical-background/fire-danger-forecast> (accessed on 11 March 2022).
42. Fotheringham, A.S.; Brunson, C.; Charlton, M. *Quantitative Geography: Perspectives on Spatial Data Analysis*, 1st ed.; Sage: London, UK, 2000; p. 288.

43. Rego, F.C.; Fernandes, P.; Sande Silva, J.; Azevedo, J.; Moura, J.M.; Oliveira, E.; Cortes, R.; Viegas, D.X.; Caldeira, D.; Duarte Santos, F. *Avaliação do Incêndio de Monchique. Relatório Observatório Técnico Independente, Comissão Técnica Independente*; Assembleia da República: Lisboa, Portugal, 2019; p. 78.
44. Cunha, S.; Silva, Á.; Herráez, C.; Pires, V.; Chazarra, A.; Mestre, A.; Nunes, L.; Mendes, M.; Neto, J.; Marques, J.; et al. *Atlas Climático Ibérico—Iberian Climate Atlas*; AEMET, Ministerio de Medio Ambiente y Medio Rural y Marino: Madrid, Spain, 2011; p. 80.
45. Rodrigues, M.; Trigo, R.M.; Vega-García, C.; Cardil, A. Identifying large fire weather typologies in the Iberian Peninsula. *Agr. Forest Meteorol.* **2020**, *280*, 107789. [[CrossRef](#)]

Disclaimer/Publisher’s Note: The statements, opinions and data contained in all publications are solely those of the individual author(s) and contributor(s) and not of MDPI and/or the editor(s). MDPI and/or the editor(s) disclaim responsibility for any injury to people or property resulting from any ideas, methods, instructions or products referred to in the content.